Preprints, 15th Symposium on Boundary Layers and Turbulence, 15-19 July, Wageningen, The Netherlands, 133-136.

REMOTE SENSING OF THE LATE-SUMMER BOUNDARY LAYER NEAR THE NORTH POLE

P. O. G. Persson[1], S. Abbott[2], M. Jensen[3], B. Larsson[4], V. Leuski[1], A. Targino[5], M. Tjernstrom[5], and A. White[1]

[1]Cooperative Institute for Research in Environmental Sciences/NOAA/ETL, Boulder, CO, USA
[2]NOAA/Environmental Technology Laboratory, Boulder, CO, USA
[3]Cooperative Institute for Research in Environmental Sciences/U. of CO, Boulder, CO, USA
[4]Infanterigatan 26A, 260 70 Ljungbyhed, Sweden
[5]Department of Meteorology, Stockholm University, 106 91 Stockholm, Sweden

1. INTRODUCTION

The Arctic atmospheric boundary layer (ABL) has been considered to be a statically stable environment generally inhibiting vertical exchange. Recent field programs (Nilsson 1996; Bigg *et al*, 1996) and modeling studies (e.g., Wang *et al*, 2000) have shown that the ABL has a complicated structure involving generally quasi-persistent, thermal and kinematic features (e.g., surface-based mixed layers, low-level jets within the stable air above, and low-level stratus clouds and fog), and more transitory features and processes often related to the quasi-persistent features. These transitory features and processes may facilitate vertical exchange. Some of the structures and processes possibly related to vertical exchange include breaking gravity waves, cloud-top cooling, surface mixed layers, horizontal roll vortices, and propagating lead-induced "microfronts". Many of these transitory features and processes occur on time scales of an hour or less.

To facilitate linking changes in atmospheric properties and aerosol concentrations to ABL structures and processes, a suite of remote sensors were deployed on the Swedish icebreaker *Oden* and on the pack ice near the North Pole during the Arctic Ocean Expedition-2001 (AOE-2001; Leck 1999) in July and August, 2001. This suite consisted of two Doppler sodars, a 915 MHz wind profiler, a scanning 5 mm radiometer, and an S-band Doppler radar. These sensors were chosen to obtain observations of the thermal, kinematic and turbulent structure in the lowest 400-1000 m of the ABL with temporal resolution of an hour or less. They complement each other well, but also have a degree of redundancy. The data from the remote sensors are validated and checked for consistency with the episodic measurements provided by a tethered balloon and kites, 6 hourly GPS rawinsondes, and the hourly surface data.

This paper will discuss the characteristics of the remote sensors and some of the data processing necessary to obtain useful data. This data processing is still ongoing. Examples of the remote sensing data in this unique environment during a 2-day period (Aug. 11-12) during the ice drift phase near 88°N will be presented to illustrate some of the capabilities of this suite of sensors. These measurements will be contrasted to the rawinsonde data, highlighting the impact of the added temporal resolution these instruments provide. The two days chosen contain a frontal passage, which produced some of the extremes in conditions encountered during the expedition, including moderate rain, snow, low clouds, and clear skies. The near-surface boundary layer contained periods of low-level stable layers, a surface mixed layer, and low-level jets (LLJs).

Corresponding author: Dr. Ola Persson, CIRES/NOAA/ETL, R/ET7, 325 Broadway, Boulder, CO 80305. email: ola.persson@noaa.gov

2. WIND AND TURBULENCE MEASUREMENTS

High temporal resolution wind and turbulence measurements were obtained with a 915 MHz boundary layer wind profiler, a vertically pointing, monostatic Doppler sodar, and a monostatic, Doppler sodar with two oblique beams.

The wind profiler was deployed on the bow of the Oden during the entire cruise. It provided measurements of wind speed, wind direction, and turbulent intensity (index of refraction structure function or C_N^2) up to 1-2 km at 60-100 m resolution every 6-60 minutes. During periods of precipitation, the range of the data was much greater. The profiler data has not been processed, yet, but it should provide a near-continuous monitoring of the LLJ and the vertical wind and turbulence structure below and above it up to near the top of the ABL. We expect it will show the onset and evolution of turbulence associated with cloud-top cooling and other processes near the top of the ABL. Normally, 1-hour averages are obtained, though higher-resolution data was saved so 6-minute values can be obtained with a loss in accuracy and sensitivity.

Both sodars had an adjustable frequency allowing the operator to select the best range for the conditions at the expense of the vertical resolution. The range was generally set at 450 - 700 m, with a resolution of 14-20 m. The vertically pointing sodar provided the vertical wind component and backscatter (due to thermal gradients) every 1-3 seconds. Stable layers will be defined by the backscatter, while the vertical wind component and its variance provide quantitative estimates of the turbulence. The processing of the data for the wind profiler and the vertically pointing sodar has just begun, and examples of these data should be available during the conference.

The two-beam, monostatic, Doppler sodar provided vertical profiles of the horizontal wind speed and backscatter every 20 seconds. Hourly mean wind profiles have been produced from this data. Future processing will provide ten-minute averages wind profiles, and we will also assess the quality of higher

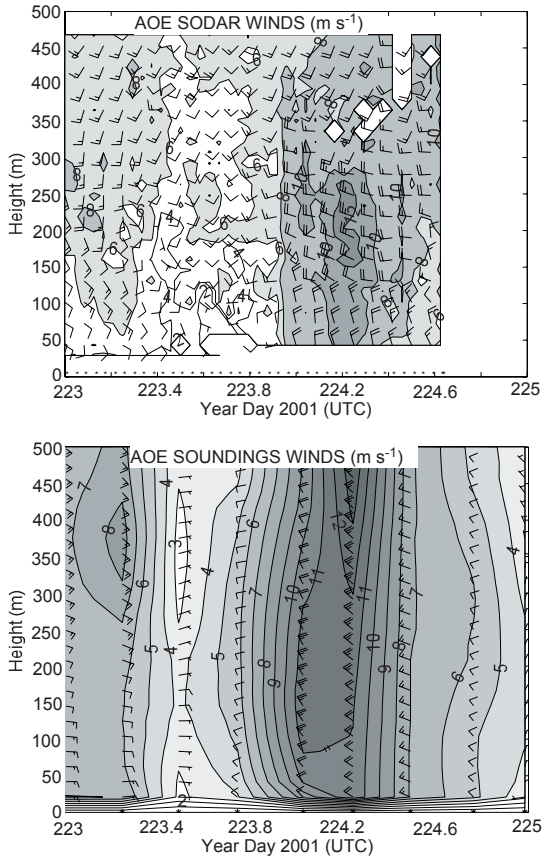

Fig. 1: Time-height sections of isotachs and wind barbs in the lowest 500 m from a) hourly-averaged data from the two-beam sodar and b) the 6-hourly rawinsondes.

resolution 1-2 minute averages. This sodar data is both redundant and complementary to the wind profiler data for monitoring the strength and variations in the LLJ. The two-beam sodar data will provide greater temporal and vertical resolution, though its range is less.

A time-height section of the winds from the two-beam sodar during our sample period shows a southerly LLJ near 200-300 m during the beginning of Julian Day (JD) 223 (Aug. 11) and a westerly LLJ at the same height about 24 hours later after the frontal passage (Fig. 1a). The sudden onset of the stronger westerly and northwesterly winds at the frontal passage near JD 223.75, supported by the hourly data from the nearby 18-m mast, is not captured by the temporally interpolated 6-hourly rawinsonde data (Fig. 1b). However, there are also other discrepancies that need to be understood. Though the strength of the two LLJs are in agreement between the sodar and the soundings, the LLJs occur at a higher altitude in the sounding data. Also, the vertical directional shear is greater in the sodar data. Vertical smoothing of the rawinsonde data may account for some of these differences, but other problems in either the sodar or the rawinsonde data may also exist. Once the wind profiler data is processed, it should be useful in resolving these discrepancies.

3. TEMPERATURE PROFILES

The 5-mm (60 GHz) scanning radiometer provided temperature profiles up to 500 m at time resolutions of 1 s to 15 minutes. The radiometer utilizes emissions in the oxygen-band of the spectrum; hence, limitations due to changing meteorological conditions don't exist. Theoretical estimates of vertical resolution are 7.5 m near the surface and 300 m near 400 m height (Westwater et al, 1999), but in practice, the resolution appears to be a factor of about 2-3 better than this. Field tests (Westwater et al, 1999) showed root-mean-square differences of less than 1 K when compared to temperature sensors on the 300-m Boulder Atmospheric Observation (BAO) tower and to rawinsondes. These comparisons included wintertime conditions in Colorado and periods of low-level stable layers. The comparisons showed that the temporal evolution at a given height below 400 m is very well represented by the radiometer. For profiles, stable layers below 500 m are somewhat smoothed but still well represented by the radiometer; stable layers at higher altitudes are very smoothed and therefore poorly represented.

During AOE, the radiometer was mounted on the top deck of the ship on the starboard (right) side, about 30 m above the ice, though having a view to both the left and right sides of the ship. It operated in a scanning mode with a period of 0.4 s. The internal reference load is connected to the receiver during 50 msec in each scanning period. The physical temperature of the reference load was measured by a thermistor and used for calibrating the radiometer. The brightness temperature as a function of rotation angle, Tb(a), is given by

$$Tb(a)=[V(a)-Vr]*G+Tr+To \ ,$$

where V(a) and Vr are output voltages corresponding to antenna and reference load states, and Tr is the physical temperature of the reference load. The two radiometer calibration coefficients, G and To, were determined by a least squares comparison of the variation of the radiometer output for a horizontal viewing direction to the left side of the ship with the air temperature during the entire 48 hour period. However, the retrieved radiometer temperatures are slightly less than those observed at the beginning and end of this period (Fig. 2). These temperature differences may be real, as they could be produced by different combinations of the wind direction, the ship orientation, the radiometer viewing direction, and heat plumes from the ship. For instance, the wind direction shifted at JD223.625 and the ship orientation was changed by 180° at JD224.5, the two times at which changes in agreement between the radiometer and the mast temperatures occurred. In addition, the mast and rawinsonde data indicated near-neutral conditions and strong winds during the middle period, and inversion conditions with weak winds before and after. Hence, the precise height of the radiometer beam relative to the other temperature measurements may also have contributed to these differences. These issues need to be addressed more closely in future analyses.

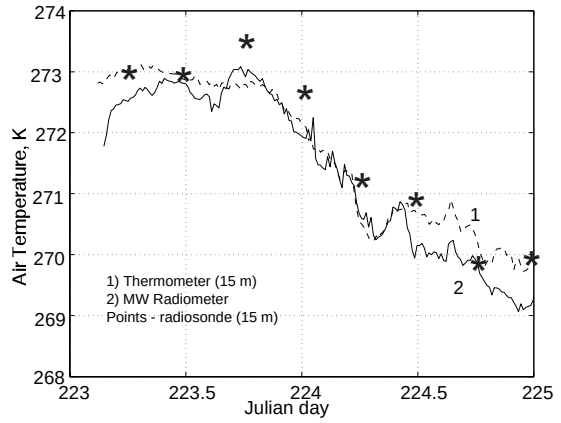

Fig. 2: Time series of Tb(0) and the 15-m temperatures from the mast and the rawinsondes.

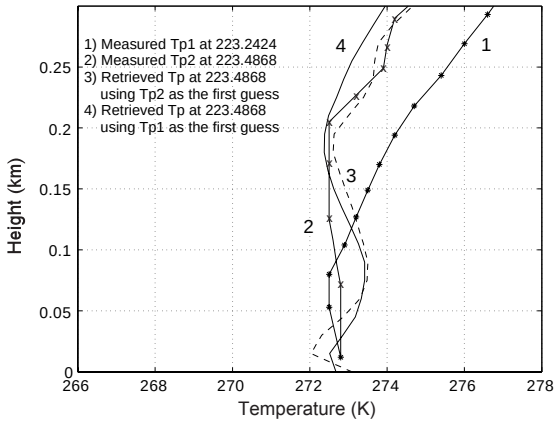

Fig. 3: Retrieved temperature profiles at 12 UTC JD223 (3 & 4) using the 06 UTC sounding (1) and the 12 UTC sounding (2) as first guesses, respectively.

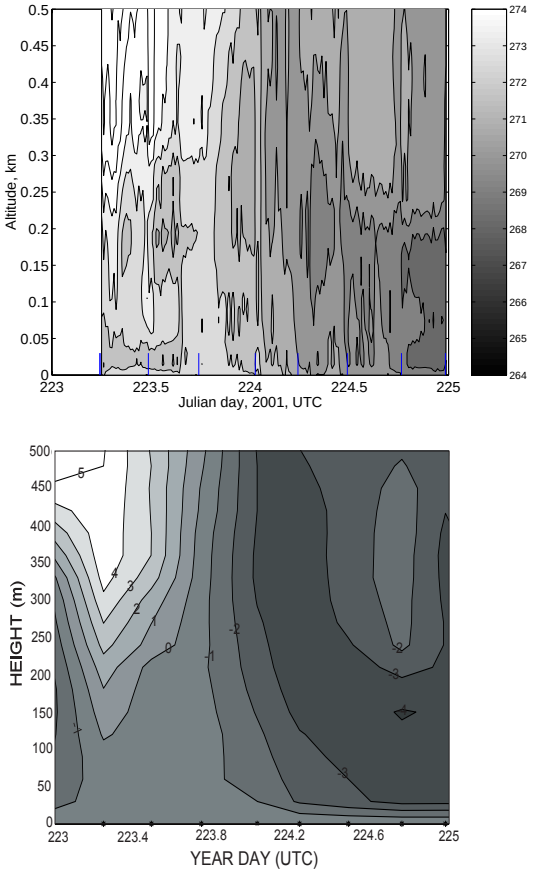

Fig. 4: Time-height sections of temperature from a) the 5-mm scanning radiometer and b) the 6-hourly rawinsondes during Aug. 11-12 (JD 223-224). The vertical bars along the x axes show the times of the rawinsonde launches.

To produce atmospheric temperature profiles, we used Rosenkranz's absorption model (Ulaby 1981) and Twomey-Tikhonov's (1996) inversion method. The temperature profile measured by the most recent radiosonde was used as a first guess in the retrieval of the temperature profiles during the time until the next radiosonde launch. Since some sensitivity to the first guess exists (Fig. 3), future refinements to the data processing may use alternative first guess profiles.

The time-height section of 15-minute retrieved temperature profiles during our two-day test period reveal several interesting thermodynamic structures and the presence of features not resolvable by the rawinsondes (Fig.4a). It shows the warm air above 250 m before the frontal passage at JD223.75, after which the cooling occurs through the entire 500 m depth. Prefrontal warm air pulses appear to penetrate to about 100 m, with a final warm pulse reaching the surface just before the frontal passage. The radiosonde data suggest a broad region of descending warm air rather than pulses (Fig. 4b). The post-frontal cooling is strongest below 250 m, reestablishing the inversion layer between 150-350 m that had been present during the earlier portions of JD223. Again, this cooling appears to occur in pulses in the radiometer data. The radiosondes do show both inversions, but the radiometer data provide a much greater amount of detail on how the inversions evolve and on transitory changes in the inversion strength. Note also that the inversion layers encompass the LLJs in the sodar data but occur below those in the sounding data.

4. CLOUDS AND PRECIPITATION

One S-band vertically pointing Doppler radar with an extended dynamic range provided reflectivity and vertical velocity within both clouds and precipitation. It used two modes with vertical resolutions of 45 and 105 m, respectively, and a temporal resolution of 30 seconds. The mode with the coarser resolution had a range of 8.5 km, while the other had a range of 2.2 km. At a range of 3 km with a 105 m resolution, its minimum detectable signal is -24.8 dBZ, while at 1 km it is -35 dBZ (White et al 2000). With 45 m resolution its minimum detectable signal is -27 dBZ at 1 km. At lower heights, the minimum detectable signal decreases exponentially. This instrument has been field tested in several experiments with excellent results, though never in the polar regions. It provided cloud outlines, cloud and precipitation reflectivity (precipitation intensity), and

spectra of particle fall speeds (which could yield information on particle phase and size). The backscatter is mostly from clouds and precipitation, with some clear-air returns. Combining the S-band data with data from a 915 MHz wind profiler provides discrimination between cloud/precipitation echoes and clear-air echoes.

The S-band radar was deployed on the bow of the *Oden* for the duration of the AOE cruise. The S-band radar data for Aug. 11-12 is available but can not be readily displayed in black and white for this paper. However, it will be displayed in color at the conference. Between 00-16 UTC on Aug. 11, the S-band data revealed cloud tops of 5-7 km**,** with precipitation occurring between 00-02 and 06 - 24 UTC. Between 02-06 UTC, the precipitation evaporated in a dry layer below 2 km (Fig. 5). After 06 UTC, significant precipitation reached the surface. The fall velocities near 11-13 UTC of > 6 ms^{-1} indicated large raindrops. As the atmosphere cooled and the freezing level descended as revealed by the bright band, the precipitation changed to snow after 18 UTC. During the period of snow, the cloud tops were at 1.5 - 4.0 km.

By 01 UTC on JD224, the snow had ended. After 06 UTC, the skies cleared, with only intermittent clouds with tops near 1 km occurring near 10-11, 1400-1730, and 1930-2200 UTC. Two short-lived clouds were also detected near 5.0-6.5 km at 0800-0830 and 23-24 UTC. The lower clouds between 1400-1730 and 1930-2200 UTC may have contained some drizzle, but the fall velocities were less than 1.5 ms^{-1} and the spectral width was less than 0.5 ms^{-1} indicating small, uniform particles. The radiosondes show the drying occurring above 1 km (Fig. 5).

After 12 UTC, the S-band radar also shows layers of weakly enhanced backscatter. The first layer oscillates between 700-1000m, with the lower height occurring between the cloudy periods and the backscatter enhancements merging with the cloud tops during the cloudy periods. A second layer is seen at 300 m height during the clear periods, but becoming obscured by the backscatter from the clouds during the cloudy periods. After the clearing near 22 UTC, this lowest layer is no longer visible. These two layers of

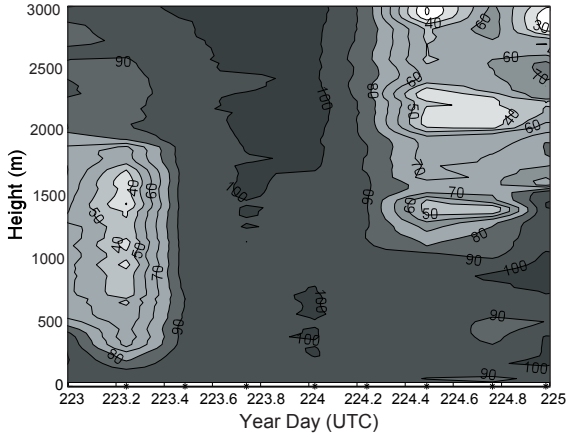

Fig. 5: Time-height section of the relative humidity with respect to ice from the rawinsondes.

weak reflectivity probably indicate a layer of enhanced turbulence with no clouds. These may signify two inversion layers with enhanced shear. The lowest one at 300 m may be the inversion layer detected by the radiometer profiles, and is seen to weaken after 20 UTC (Fig. 4). Again, as for the other remote sensors, the detail revealed by the S-band radar is far beyond that possible from the rawinsonde data, despite the relatively good temporal resolution of the latter.

5. FUTURE USE

This paper illustrates some of the potential in the remote sensing data collected during the AOE-2001 field program. To illustrate the capabilities of the instruments, data from the two-beam sodar, the 5-mm scanning radiometer, and the S-band Doppler radar have been discussed during a very active and varying two day period. Data is also available from the vertically pointing monostatic sodar and the 915 MHz wind profiler. The processing of the data continues, with a completion of the initial processing expected in fall of 2002. It is hoped that the future analysis of this unique and rich data set will provide a better understanding of the process in the late-summer boundary layer over the Arctic pack ice.

REFERENCES

Bigg, E. K., C. Leck, and E. D. Nilsson, 1996: Sudden changes in arctic atmospheric aerosol concentration during summer and autumn. *Tellus*, **48B**, 254-271.

Leck, C., E. Swietlicki, E. K. Bigg, M. Tjernström, M. Kulmala, and P. Wassman, 1999: The Atmospheric Research Program of the Arctic Ocean Expedition in the Summer of 2001. Science and Implementation Plan. [Available from Dept. of Meteorology, University of Stockholm, S-106 91, Stockholm, Sweden. E-mail lina@misu.su.se]

Nilsson, E. D., 1996: Planetary boundary layer structure and air mass transport during the International Arctic Ocean Expedition 1991. *Tellus*, **48B**, 178-196.

Twomey, S., *"Introduction to the Mathematics of Inversion in Remote Sensing and Indirect Measurements"*, New York, Dover Publication Inc. 1996

Ulaby, F. T., R.K.Moore,A.K.Fung, "*Microwave Remote Sensing",* v.1. Artech House, MA.1981

Westwater, E., Y. Han, V. G. Irisov, V. Leuskiy, E. N. Kadygrov, and S. A. Viazankin, 1999: Remote sensing of boundary layer temeprature profiles by a scanning 5-mm microwave radiometer and RASS: Comparison experiments. *J. Atmos. Ocean. Tech.*, **16**, 805-818.

White, A.B., J. Jordan, B. Martner, F. Ralph and B. Bartram, 2000: Extending the dynamic range of an S-band radar for cloud and precipitation studies. *J. Atmos. Ocean. Tech.*, **17**,1226-1234.

Wang, S., Q. Wang, R. E. Jordan, and P. O. G. Persson, 2001: Interactions among longwave radiation of clouds, turbulence and snow surface temperature in the Arctic: A model sensitivity study. J. Geophys. Res 106 (D14), 15,323-15,333.